HHS Public Access

Author manuscript

Anal Methods. Author manuscript; available in PMC 2018 February 07.

Published in final edited form as:

Anal Methods. 2017 February 7; 9(5): 847–855. doi:10.1039/C6AY03342C.

Microfluidic Iterative Mechanical Characteristics (iMECH) Analyzer for Single-Cell Metastatic Identification

Hesam Babahosseini[a,b], **Jeannine S. Strobl**[b], and **Masoud Agah**[b,*]

[a]Department of Mechanical Engineering, Virginia Tech, Blacksburg, VA 24061, US

[b]The Bradley Department of Electrical and Computer Engineering, Virginia Tech, Blacksburg, VA 24061, US

Abstract

This study describes the development of a microfluidic biosensor called the iterative mechanical characteristics (iMECH) analyzer which enables label-free biomechanical profiling of individual cells for distinction between metastatic and non-metastatic human mammary cell lines. Previous results have demonstrated that pulsed mechanical nanoindentation can modulate the biomechanics of cells resulting in distinctly different biomechanical responses in metastatic and non-metastatic cell lines. The iMECH analyzer aims to move this concept into a microfluidic, clinically more relevant platform. The iMECH analyzer directs a cyclic deformation regimen by pulling cells through a test channel comprised of narrow deformation channels and interspersed with wider relaxation regions which together simulate a dynamic microenvironment. The results of the iMECH analysis of human breast cell lines revealed that cyclic deformations produce a resistance in non-metastatic 184A1 and MCF10A cells as determined by a drop in their average velocity in the iterative deformation channels after each relaxation. In contrast, metastatic MDA-MB-231 and MDA-MB-468 cells exhibit a loss of resistance as measured by a velocity raise after each relaxation. These distinctive modulatory mechanical responses of normal-like non-metastatic and metastatic cancer breast cells to the pulsed indentations paradigm provide a unique bio-signature. The iMECH analyzer represents a diagnostic microchip advance for discriminating metastatic cancer at the single-cell level.

TOC Image

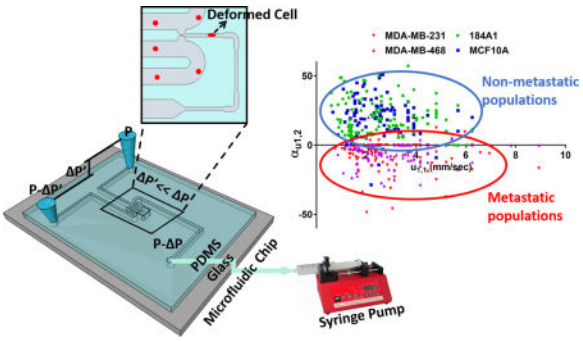

*Corresponding author: agah@vt.edu.

Keywords

cell mechanics; single-cell analysis; microfluidics chip; breast cancer

Introduction

Mechanical factors can direct cellular growth, function and homeostasis, but also cause or contribute to diseases such as cancer. The biomechanical properties of cells are modulated in response to their environmental factors and are thereby linked to physiological and pathophysiological functions.[1] To date, biomechanical properties have gained broad acceptance in cell biology as a highly sensitive, label-free, non-destructive method for determining the health state of cell without the use of fluorescent, magnetic, or other cell markers. The biomechanical properties of cancer cells are constantly changing during progression of tumors to more aggressive and metastatic type[2] and progression is accompanied by alterations in the levels of expression of biochemical factors and regulators of cytoskeletal organization, which impact cell migration, adherence, and invasion.[3, 4] Thus, the ability to characterize the biomechanical nature of a cell could provide novel insights into how cells receive and integrate regulatory signals from the surrounding environment which can impact disease progression diagnosis and treatment. There are currently different instruments and methods available for assessing cell biomechanical properties.[5, 6] There have been a handful of reports quantifying the changes take place in cellular biomechanical properties during the metastatic process.[6] In general, the progression of cancer is associated with an alteration of the cell structure which in turn causes transformed cells to be softer and hence more deformable than their healthier counterparts to facilitate metastasis.[7–9] The investigations have also showed that reduced surface friction of cancer cells may play another important role in further facilitating the motility.[10, 11]

The development of microfluidic devices for biomarker detection and point-of-care disease diagnosis has been on the rise because of their remarkable features including simplicity, low-cost, and high-speed.[12–14] Among its potential uses for different disease diagnosis, prototypes to elucidate cancer cell and tumor function have gained tremendous importance.[15, 16] Microfluidic-based analyzers for cell biomechanical screening and mechanophenotyping have promised a higher throughput compared to conventional tools and emerged as a clinically more relevant approach to single-cell analysis.[17–20] As an important note, single-cell level analysis in cancer diagnosis is a critical need in light of the knowledge that tumor masses are comprised of a heterogeneous mixture of cells.[21] Single-cell level analysis can significantly contribute to the evolution in the diagnostic and prognostic decisions to cancer patients.[22, 23] Currently, several microfluidic constriction channel based analyzers have been developed for quantitative biomechanical characterizations of various cell types including tumor cells, red blood cells (RBCs), and white blood cells (WBCs). (Table 1)

Nevertheless, most endeavors in cell biomechanical characterizations have typically utilized single-pulse transient mechanical stimulus for mechanophenotyping and cellular mechanical responses analysis.[57, 58] These measurements reveal differences in the biomechanical

properties of normal and cancer at the population level, but quantified parameters thus far defined cannot predict whether a given individual cell is malignant or normal. Accurate cell biomechanical characterization involves cell investigation in simulated realistic environments as living cells can sense external environmental loads and respond to them by adapting their structure.[59] Some researchers have made attempts to mimic the physiological microenvironments of cells where they undergo dynamic mechanical stimuli. Particularly, cancer cells are exposed to continuous time-varying shear stresses as a result of the elevated interstitial fluid flow. These shear stresses can alter cancer cytophysiology in ways that support cancer cell invasiveness.[60] Some studies have reported different responses of normal and cancer cells to such dynamic stressors even under artificial dynamic microenvironment shifts. As reported, cell stiffness of non-tumorigenic/normal cells increases in response to dynamic stress/strain. For instance, it has been shown that normal cells stiffen during tapping motions imposed by an atomic force microscopy (AFM) cantilever probe and these cells become less susceptible to deformation.[61] In another study, rapid stretch of adherent normal endothelial cells resulted in a quick increase in actin lattice stiffness, and thus mechanical resistance.[62] Furthermore, Mak et al. developed a microfluidic device and showed a decrease in the measured transit times of invasive MDA-MB-231 breast cells under a sequence of deformations through serial subnucleus-scaled constriction channels.[24, 25] The conclusion from this work was that the MDA-MB-231 cells underwent mechanical compliance.

Our group has recently produced solid evidence indicating that metastatic and non-metastatic single cells respond differently to nanomechanical indentations applied to them in a pulsed mode.[63] According to that study, the non-metastatic MCF10A and 184A1 cells increased their resistance against deformation while metastatic cells became slightly softer when subjected to a dynamic mechanical microenvironment. Our aim here is to transition principles gained by the AFM technique[63] into a suitable single-cell analysis platform on a high-throughput microfluidic chip. To this end, the microfluidic iterative mechanical characteristics (iMECH) analyzer has been developed and its ability to reveal unique information about the health status of single cells is demonstrated.

Materials and Methods

Cell Culture and Treatment

The microfluidic iMECH analyzer's performance as a biosensor was evaluated using four breast cancer cell lines including immortalized, non-tumorigenic, non-metastatic 184A1 and MCF10A cells and tumorigenic, metastatic MDA-MB-468 and MDA-MB-231 cells (All cell lines were purchased from ATCC; American Type Culture Collection, Manassas, VA). The standard culture medium for 184A1 cell growth was MEGM kit supplemented with 5 μg/ml transferrin (Sigma Aldrich, St. Louis, MO) and 1 ng/ml cholera toxin (Lonza, Basel, Switzerland); the gentamycin-amphotericin B was omitted. MCF10A cells were grown in F12:DMEM (Lonza, Basel, Switzerland) with penicillin-streptomycin (100 Units/ml), 2.5 mM L-glutamine, 20 ng/ml epidermal growth factor (EGF), 0.1 μg/ml cholera toxin (CT), 10 μg/ml insulin, 0.5 μg/ml hydrocortisone, and 5% horse serum. MDA-MB-468 cells were grown in L-15 supplemented with 10% fetal bovine serum (FBS), 4 mM glutamine and

penicillin-streptomycin (100 Units/ml). Finally, MDA-MB-231 cells were grown in F12:DMEM with 10% FBS, 4 mM glutamine and penicillin-streptomycin (100 Units/ml). The cells were suspended in culture medium at a concentration of 5×10^5 cells/mL for delivery into the iMECH analyzer.

Microchip Design and Fabrication

The iMECH analyzer consists of a multi-segmented test channel which mimics a dynamic deformation paradigm and a U-shaped delivery channel (200 μm-wide and 60 μm-deep). The test channel contains three deformation channels (6 μm-wide, 12 μm-deep, 500 μm-long) separated by two relaxation regions (30μm-wide, 30μm-deep, 100μm-long). The design of the iMECH analyzer is depicted schematically in Figure 1A. To deliver single cells to the test channel, a free flow of suspended cells in culture medium is established in the delivery channel by the height difference of medium in the reservoirs at the inlet/outlet ports. Single cells are trapped and pulled into the test channel by applying a negative pressure ($\Delta P=-150$ Pa) via a syringe pump (Harvard apparatus, Holliston, MA) at the end of the test channel. A trapping mechanism adapted from a work by Tan et al.[64] based on hydrodynamic resistance at the entrance of the test channel helps the single cell trapping. As cells pass through the test channel, they undergo a series of deformation and relaxation events as they pass through deformation and relaxation regions. The information about the modulatory biomechanical properties of single cells in response to this dynamic microenvironment in the microchip is collected, resulting in the single-cell iMECH bio-signature. The velocity of individual cells in the deformation channels is measured and used as an indicator of cell biomechanics. The iMECH analyzer enables the analysis of about 1 cell/sec without sacrificing the sensitivity of the system to discriminate between the biomechanical behavior of metastatic and non-metastatic cells.

The iMECH analyzer was fabricated in the clean room facility. A master wafer was initially fabricated using a two-step etching process to obtain the shallow constriction channel and the deep delivery channel. Briefly, a thin photoresist (Shipley 1827) was spun coated on a silicon wafer and patterned using photolithography. A shallow etch was done using deep reactive ion etching (DRIE, Bosch, Germany) for a depth of 12 μm. The photoresist was stripped before a second round of photolithography using a thicker photoresist (AZ9260) to fabricate the delivery channel. The wafer was etched for 20 min in the DRIE to obtain an overall depth of 30 μm. Finally, the photoresist was stripped and the wafer was cleaned before a layer of saline was evaporated on the wafer to enable easy peel-off of polydimethylsiloxane (PDMS). PDMS prepolymer and curing agent were mixed at a ratio of 10:1, poured over the silicon master placed in an aluminum foil plate, degassed in a vacuum desiccators to remove air bubbles, and baked in a convection oven (15 min, 125°C). The device was allowed to cool, then peeled off from the master, diced and reservoir holes were punched through. At the end, the PDMS layer and a glass slide were concurrently treated with oxygen plasma in a plasma cleaner (Harrick Plasma, Plasma Cleaner) for 1 min and bonded together. The fabrication process of the iMECH analyzer is shown step by step in Figure 1B. A schematic of the iMECH setup and operation principles is shown in Figure 1C.

Data Acquisition and Analysis

For data acquisition, the device was mounted onto the Zeiss Axio Observer inverted microscope (Carl Zeiss, Jena, Germany). The video images of the cells passing through the test channel were recorded via Motion Xtra NX4-S3 high speed camera (IDT, Tallahassee, FL) with 5 GB memory and Motion Studio software at 500 frames per second. To examine and validate the reproducibility and consistency of the results, at least three separate tests were conducted for each cell population with at least n=100 cells from each sample. Within the same cell population, there was no more than 5% variation between the average measured parameters of any two reported test results. *P*-values between the different populations were calculated using two independent samples t-tests ($\alpha = 0.05$). Results are presented as arithmetic mean ± standard error of the mean (SEM) using GraphPad Prism software.

Results and discussion

Cell Mechanical Characteristics in Micro-channels

The cell movement in the deformation channel is driven by a pressure gradient applied across two sides of the deformation channels. The two-dimensional plot of the pressure gradient in the microfluidic channels is simulated in COMSOL Multiphysics and is shown in Figure 2A. It can be seen that the pressure gradients across the narrow deformation channels are equal and about ΔP=−40 Pa. It implies that the cells are experiencing the same applied pulling pressure across each deformation channel. Importantly, 4 μm beads passed through the test channel showed equal traveling times in all three deformation channels. It indicates that the deformation channels were fabricated with an identical size and cross section and the beads experience an equal pressure gradient across them. Cell velocity in the deformation channels was measured visually and by a developed MATLAB code using the obtained image videos. A cell's movement in the deformation channel can be separated into two phases as shown previously;[48] during phase I, the cell moves with a non-constant velocity when undergoing a heavy deformation within the narrow deformation channel and during phase II, the cell velocity remains constant when reaching a steady state. Figure 2B shows a schematic profile of location versus time for a cell in a deformation channel.

Analysis of the cell movements in the deformation channels revealed that the transition point between phase I (non-constant velocity) and phase II (constant velocity) always occurred in the first-half of the 500 μm deformation channels. For our analysis, we divided the deformation channels into two halves: the transient and equilibrium sections. The corresponding average velocities of transient and equilibrium sections ($u_{i,1}$ and $u_{i,2}$, respectively) of the deformation channels (i=1, 2, 3) are depicted in Figure 2A. The average transient and equilibrium velocities of the iterative deformation channels for a typical non-metastatic and metastatic cell are depicted in Figure 2C and 2D, respectively. The average velocities for the cells subjected to iterative mechanical deformations through the deformation channels revealed that the non-metastatic cells exhibit a velocity drop after each relaxation region once they enter to the next deformation channel as shown in Figure 2C. The drop in the average transient velocity of the non-metastatic cells after a recovery period afforded by passage through a wider channel interspersed between each deformation channel

can be due to the effect of mechanical resistance in their structural characteristics in response to iterative deformations. However, this trend is reversed in the metastatic cells. After each relaxation region, the average transient velocity of the metastatic cells rises or remains constant as cells proceed to enter subsequent deformation channels (Figure 2D). It implies that the metastatic cells averagely exhibit a mechanical compliance with iterative deformations in their structure.

Cell iMECH Bio-Signature

The average transient and equilibrium velocity measurements of breast cell type populations are presented in Figure 3A. MDA-MB-231 and MDA-MB-468 metastatic cells showed 5% and 4% increases in the average velocities from $u_{1,2}$ to $u_{2,1}$ and also 4% and 4% increases from $u_{2,2}$ to $u_{3,1}$, respectively. Therefore, these data are suggestive that the representative metastatic cells slightly lose their mechanical resistance to travel through narrow channels in response to iterative deformations by increasing in their transient velocities after the first and second deformation channels. In contrast, the representative non-metastatic cells responded by decreasing in their transient velocities after each deformation channels. the average velocity of 184A1 and MCF10A cells decreased by ~21% and ~20% from $u_{1,2}$ to $u_{2,1}$ and ~8% and ~6% from $u_{2,2}$ to $u_{3,1}$, respectively. These data imply that non-metastatic cell behavior is the reverse of that seen in the metastatic cells and that these cells show a rise in their mechanical resistance to travel through the deformation channel.

Here, we define the relative percentage changes of velocity (α_u) for individual cells as the average equilibrium velocity in one deformation channel compared to the average transient velocity in the next deformation channel ($\alpha_{u\ i,i+1} = (u_{i,2}-u_{i+1,1})/u_{i,2}$) for i=1, 2). The relative percentage change of velocity is used as an index for examining the modulation in the mechanical resistance of cells. The α_u between each two successive deformation channels for the four cell types was calculated and is depicted by the column bars in Figures 3B.

In accordance with the results in Figure 3A, the average values of α_u for both non-metastatic cell lines were positive at each two successive deformation channels (Figure 3B), substantiating the idea that these cell lines exhibit a continuous mechanical resistance response against deformations. Importantly, the average values of α_u for the two non-metastatic cell lines appreciably reveal decreasing trends from $\alpha_{u1,2}$ to $\alpha_{u2,3}$. These data indicate that the mechanical resistance trend in the non-metastatic cells drops sharply after the initial deformation. Moreover, the average α_u values for metastatic cell lines (Figure 3B) are both negative. It is also remarkable that the average $\alpha_{u1,2}$ is larger than the average $\alpha_{u2,3}$ in the both metastatic cells, suggesting that the greatest degree of cell mechanical compliance occurred at the initial deformation.

We also examined the α_u values of individual cells; only 6% and 4% of all tested MCF10A and 184A1 cells, respectively, whose $u_{1,1}$ velocity were relatively close to the average velocity of the metastatic cells, did not show a positive number in $\alpha_{u1,2}$. In addition, 71% and 67% of MCF10A and 184A1 cells showed positive values for $\alpha_{u2,3}$, respectively. There are non-metastatic cells that have positive values for both $\alpha_{u1,2}$ and $\alpha_{u2,3}$ parameters which can be labeled with some confidence as sub-populations with a persistent mechanical resistance. Accordingly, 67% and 65% of MCF10A and 184A1 cells fall into the persistent

resistance sub-populations. Therefore, the majority of non-metastatic cells exhibited some degree of mechanical resistance in response to the iterative deformations.

At the single-cell level of the metastatic cells, 91% and 93% of MDA-MB-231 and MDA-MB-468 cells, have negative/zero values for their $\alpha_{u1,2}$, respectively. Also, 84% and 85% of MDA-MB-231 and MDA-MB-468 cells have negative/zero values for their $\alpha_{u2,3}$, respectively. There is a sub-population of 78% of MDA-MB-231 and 80% of MDA-MB-468 cells that exhibit a persistent mechanical compliance as measured by negative/zero values for both $\alpha_{u1,2}$ and $\alpha_{u2,3}$. More importantly, only 4% and 3% of MDA-MB-231 and MDA-MB-468 cells were observed to exhibit a persistent positive value in both of their $\alpha_{u1,2}$ and $\alpha_{u2,3}$, respectively. Therefore, the populations of non-metastatic and metastatic cells can begin to be identified by the trend of their modulatory mechanical behaviors in response to an iterative deformations paradigm.

According to the results in Figure 3B, the relative percentage change of velocity between two initial successive channels ($\alpha_{u1,2}$) provides a more distinct and sensitive index for differentiation between non-metastatic and metastatic cells. Thus, only two successive deformation channels in this design might be enough to discriminate between metastatic and non-metastatic cells with single-cell resolution. Together, these distinct modulatory responses of metastatic and non-metastatic cells to dynamic mechanical stimuli provided a proof-of-principle for the significance of our proposed iMECH bio-signature.

Single-Cell Level Identification using iMECH Bio-Signature

Figure 4A shows a scatter plot of every individual cell's average transient velocity versus equilibrium velocity corresponding to the first deformation channel ($u_{1,1}$, $u_{1,2}$). It is equivalent to the results extracted from a single-pulse mechanical stimulus, typically utilized for cell biomechanical characterizations. Figure 4A clearly illustrates inadequacy of using a single-pulse mechanical deformation to differentiate non-metastatic and metastatic cells at single-cell level due to a significant overlap in their measured $u_{1,1}$ and $u_{1,2}$. Therefore, a single microfluidic constriction channel typically used for measuring difference in the biomechanical properties of cells, although effective at population-level, cannot differentiate malignancy or normalcy between cell types at the single-cell level. Our hypothesis that non-metastatic and metastatic cells show overall opposite trends in adjusting their mechanical resistance under an iterative deformations paradigm suggested that incorporation of the relative change of velocity (α_u) for the individual cells through consecutive deformation channels rather than their absolute velocity provides a more effective biomarker to label single cells.

The scatter plot of the relative percentage change of velocity between two initial deformation channels ($\alpha_{u1,2}$) vs. the first deformation channel's absolute transient velocity ($u_{1,1}$) for the individual tested cells are depicted in Figure 4B. These data again show that a new mechanical descriptor of a non-metastatic cell can be defined as having positive values for $\alpha_{u1,2}$, and for a metastatic cell is defined as having one negative/zero value for $\alpha_{u1,2}$. Using these definitions, about 95% of the non-metastatic (normal-like) cells (94% of MCF10A cells and 96% of 184A1 cells) and about 92% of the metastatic cancer cells (91%

of MDA-MB-231 cells and 93% of MDA-MB-468 cells) and overall, about 93% of all tested cells are classified as non-metastatic or metastatic.

In summary, dynamic behaviors of subcellular fibrous proteins and cytoskeleton network remodeling induced by periodic stretch or compression were previously reported.[65–70] Here, we defined a unique bio-signature by evaluating and quantifying this dynamic biomechanical characteristic of individual cells for distinguishing between non-metastatic (normal-like) and metastatic cancer cells with a high confidence level.

iMECH Bio-Signatures of Mixed Cell Line Populations

In another set of experiments, the iMECH analyzer was used for testing different mixtures of metastatic MDA-MB-231 and non-metastatic MCF10A cells with ascending ratio. The percentage of tested cells from each mixture that are identified as metastatic cells using the iMECH bio-signature ($\alpha_{u1,2}$) are reported in Table 2. For each test and reported percentage, three replicates were performed. As expected, as the ratio of metastatic MDA-MB-231 to non-metastatic MCF10A cells in the mixture increased, the percentage of tested cells in the mixture recognized as potential metastatic cells based on iMECH bio-signature gradually increased. As a note, when there were no MDA-MB-231 cells in the “mixture”, about 7% were identified as metastatic; this is a measure of the false positive rate of this indicator. When the mixture contained 100% MDA-MB-231 cells, 95% of cells were identified as metastatic, indicating that the false negative rate for predicting the presence of a metastatic cells is about 5%.

Conclusion

A biosensing microfluidic chip was developed in this work to provide iterative mechanical characteristics (iMECH) of human breast cells in response to a dynamic microenvironment. The described iMECH microfluidic device, the first of its kind, provides a low-cost yet high-throughput for single-cell level metastatic detection. In summary, as cells pass through successive deformation/relaxation regions, the resistance of metastatic cells decreased while that of the non-metastatic cells increased after each relaxation period. Hence, two populations can be differentiated from one another based upon their dynamic behavior even if the two populations produce the same velocity in the first deformation channel. The described iMECH microchip makes the modulatory biomechanical behavior of cells a readily available label-free biomarker to be able to identify metastatic cells from non-metastatic cells. In the future, the iMECH analyzer may provide instrumentation enabling novel ways for detecting metastatic cells in clinical samples and also drug screening.

Acknowledgments

This research is supported by the National Science Foundation (NSF) under award number CBET-1403304 and by the National Institute of Health (NIH) under award number 1R21CA210126-01. We acknowledge the Micro & Nano Fabrication Laboratory at Virginia Tech for equipment support.

Notes and References

1. Hoffman BD, Crocker JC. Annu Rev Biomed Eng. 2009; 11:259–288. [PubMed: 19400709]

2. Lambrechts A, Van Troys M, Ampe C. Int J Biochem Cell Biol. 2004; 36:1890–1909. [PubMed: 15203104]
3. Wirtz D, Konstantopoulos K, Searson PC. Nat Rev Cancer. 2011; 11:512–522. [PubMed: 21701513]
4. Kumar S, Weaver VM. Cancer Metastasis Rev. 2009; 28:113–127. [PubMed: 19153673]
5. Di Carlo D. J Lab Autom. 2012; 17:32–42. [PubMed: 22357606]
6. Suresh S. Acta Biomater. 2007; 3:413–438. [PubMed: 17540628]
7. Ward KA, Li WI, Zimmer S, et al. Biorheology. 1991; 28:301–313. [PubMed: 1932719]
8. Swaminathan V, Mythreye K, OBrien ET, Berchuck A, Blobe GC, Superfine R. Cancer Res. 2011; 71:5075–5080. [PubMed: 21642375]
9. Xu W, Mezencev R, Kim B, Wang L, McDonald J, Sulchek T. PLoS One. 2012; 7:e46609. [PubMed: 23056368]
10. Byun S, Son S, Amodei D, Cermak N, Shaw J, Kang JH, Hecht VC, Winslow MM, Jacks T, Mallick P, Manalis SR. Proc Natl Acad Sci USA. 2013; 110:7580–7758. [PubMed: 23610435]
11. Gabriele S, Benoliel AM, Bongrand P, Theodoly O. Biophys J. 2009; 96:4308–4318. [PubMed: 19450501]
12. Sanjay ST, Fu G, Dou M, Xu F, Liu R, Qi H, Li X. Analyst. 2015; 140:7062–7081. [PubMed: 26171467]
13. Valizadeh A, Yari Khosroushahi A. Anal Methods. 2015; 7:8524–8533.
14. Zhang W, Guo S, Carvalho WSP, Jiang Y, Serpe MJ. Anal Methods. 2016; 8:7847–7867.
15. Pappas D. Analyst. 2016; 141:525–535. [PubMed: 26579548]
16. Zhang JZ, Nagrath S. Biomed Microdevices. 2013; 15:595–609. [PubMed: 23358873]
17. Xue C, Wang J, Zhao Y, Chen D, Yue W, Chen J. Micromachines. 2015; 6:1794–1804.
18. Zheng Y, Nguyen J, Wei Y, Sun Y. Lab Chip. 2013; 13:2464–2483. [PubMed: 23681312]
19. Perez-Gonzalez VH, Gallo-Villanueva RC, Camacho-Leon S, Gomez-Quinones JI, Rodriguez-Delgado JM, Martinez-Chapa SO. IET Nanobiotechnology. 2016; 10:263–275. [PubMed: 27676373]
20. Chaudhuri PK, Ebrahimi Warkiani M, Jing T, Kenry, Lim CT. Analyst. 2016; 141:504–524. [PubMed: 26010996]
21. Meacham CE, Morrison SJ. Nature. 2013; 501:328–337. [PubMed: 24048065]
22. Chen XX, Bai F. Cancer Biol Med. 2015; 12:184–192. [PubMed: 26487963]
23. Navin NE. Cancer Res. 2016; 76:1305–1312. [PubMed: 26941284]
24. Mak M, Erickson D. Integr Biol. 2013; 5:1374–1384.
25. Mak M, Reinhart-King CA, Erickson D. Lab Chip. 2013; 13:340–348. [PubMed: 23212313]
26. Hou HW, Li QS, Lee GYH, Kumar AP, Ong CN, Lim CT. Biomed Microdevices. 2009; 11:557–564. [PubMed: 19082733]
27. Khan ZS, Vanapallia SA. Biomicrofluidics. 2013; 7:011806.
28. Babahosseini H, Srinivasaraghavan V, Zhao Z, Gillam F, Childress E, Strobl JS, Santos WL, Zhang C, Agah M. Lab Chip. 2016; 16:188–198. [PubMed: 26607223]
29. Lange JR, Steinwachs J, Kolb T, Lautscham LA, Harder I, Whyte G, Fabry B. Biophys J. 2015; 109:26–34. [PubMed: 26153699]
30. Lee LM, Liu AP. Lab Chip. 2015; 15:264–273. [PubMed: 25361042]
31. Ilyas A, Asghar W, Ahmed S, Lotan Y, Hsieh JT, Kim YT, Iqbal SM. Anal Methods. 2014; 6:7166–7174.
32. Guan G, Chen PCY, Peng WK, Bhagat AA, Ong CJ, Han J. J Micromech Microeng. 2012; 22:105037.
33. Adamo A, Sharei A, Adamo L, Lee BK, Mao S, Jensen KF. Anal Chem. 2012; 84:6438–6443. [PubMed: 22746217]
34. Chen J, Zheng Y, Tan Q, Zhang YL, Li J, Geddie WR, Jewett MAS, Sun Y. Biomicrofluidics. 2011; 5:14113. [PubMed: 21523251]
35. Chen J, Zheng Y, Tan Q, Shojaei-Baghini E, Zhang YL, Li J, Prasad P, You L, Wu XY, Sun Y. Lab Chip. 2011; 11:3174–3181. [PubMed: 21826361]

36. Zheng Y, Shojaei-Baghini E, Azad A, Wang C, Sun Y. Lab Chip. 2012; 12:2560–2567. [PubMed: 22581052]
37. Huang S, Undisz A, Diez-Silva M, Bow H, Dao M, Han J. Integr Biol. 2013; 5:414–422.
38. Bow H, Pivkin IV, Diez-Silva M, Goldfless SJ, Dao M, Niles JC, Suresh S, Han J. Lab Chip. 2011; 11:1065–1073. [PubMed: 21293801]
39. Guo Q, Reiling SJ, Rohrbach P, Ma H. Lab Chip. 2012; 12:1143–1150. [PubMed: 22318405]
40. Guo Q, Park S, Ma H. Lab Chip. 2012; 12:2687–2695. [PubMed: 22622288]
41. Kwan JM, Guo Q, Kyluik-Price DL, Ma H, Scott MD. Am J Hematol. 2013; 88:682–689. [PubMed: 23674388]
42. Guo, Quan, Duffy, Simon P., Matthews, Kerryn, Santoso, Aline T., Scott, Mark D., Ma, Hongshen. J Biomech. 2014; 47:1767–1776. [PubMed: 24767871]
43. Santoso AT, Deng X, Lee JH, Matthews K, Duffy SP, Islamzada E, McFaul SM, Myrand-Lapierre ME, Ma H. Lab Chip. 2015; 15:4451–4460. [PubMed: 26477590]
44. Myrand-Lapierre ME, Deng X, Ang RR, Matthews K, Santoso AT, Ma H. Lab Chip. 2015; 15:159–167. [PubMed: 25325848]
45. Shelby JP, White J, Ganesan K, Rathod PK, Chiu DT. Proc Natl Acad Sci USA. 2003; 100:14618–14622. [PubMed: 14638939]
46. Herricks T, Antia M, Rathod PK. Cell Microbiol. 2009; 11:1340–1353. [PubMed: 19438513]
47. Quinn DJ, Pivkin I, Wong SY, Chiam KH, Dao M, Karniadakia GE, Suresh S. Ann Biomed Eng. 2011; 39:1041–1050. [PubMed: 21240637]
48. Tsai CHD, Sakuma S, Arai F, Kaneko M. IEEE Trans Biomed Eng. 2014; 61:1187–1195. [PubMed: 24658243]
49. Handayani S, Chiu DT, Tjitra E, Kuo JS, Lampah D, Kenangalem E, Renia L, Snounou G, Price RN, Anstey NM, Russell B. J Infect Dis. 2009; 199:445–450. [PubMed: 19090777]
50. Lee WG, Bang H, Yun H, Lee J, Park J, Kim JK, Chung S, Cho K, Chung C, Han DC, Chang JK. Lab Chip. 2007; 7:516–519. [PubMed: 17389970]
51. Abkarian M, Faivre M, Stone HA. Proc Natl Acad Sci USA. 2006; 103:538–542. [PubMed: 16407104]
52. Gabriele S, Versaevel M, Preira P, Theodoly O. Lab Chip. 2010; 10:1459–1467. [PubMed: 20480111]
53. Preira P, Valignat MP, Bico J, Theodoly O. Biomicrofluidics. 2013; 7:024111.
54. Lam WA, Rosenbluth MJ, Fletcher DA. Blood. 2007; 109:3505–3508. [PubMed: 17179225]
55. Rosenbluth MJ, Lam WA, Fletcher DA. Lab Chip. 2008; 8:1062–1070. [PubMed: 18584080]
56. Yap B, Kamm RD. J Appl Physiol. 2005; 98:1930–1939. [PubMed: 15640383]
57. Hoffman BD, Grashoff C, Schwartz MA. Nature. 2011; 475:316–323. [PubMed: 21776077]
58. Babahosseini H, Strobl JS, Agah M. Nanomedicine. 2015; 10:2635–2638. [PubMed: 26328619]
59. Bao G, Suresh S. Nature Materials. 2003; 2:715–725. [PubMed: 14593396]
60. Munson JM, Shieh AC. Cancer Manag Res. 2014; 6:317–328. [PubMed: 25170280]
61. Putman CAJ, Van der Werf KO, De Grooth BG, Van Hulst NF, Greve J. Biophys J. 1994; 67:1749–1753. [PubMed: 7819507]
62. Pourati J, Maniotis A, Spiegel D, Schaffer JL, Butler JP, Fredberg JJ, Ingber DE, Stamenovic D, Wang N. Am J Physiol. 1998; 274:C1283–1289. [PubMed: 9612215]
63. Babahosseini H, Strobl SS, Agah M. Nanotechnology. 2015; 26:354004. [PubMed: 26266760]
64. Tan WH, Takeuchi S. Proc Natl Acad Sci U S A. 2007; 104:1146–1151. [PubMed: 17227861]
65. Hsu HJ, Lee CF, Kaunas R. PLoS ONE. 2009; 4:e4853. [PubMed: 19319193]
66. Liu B, Qu MJ, Qin KR, Li H, Li ZK, Shen BR, Jiang ZL. Biophys J. 2008; 94:1497–1507. [PubMed: 17993501]
67. Icard-Arcizet D, Cardoso O, Richert A, Henon S. Biophys J. 2008; 94:2906–2913. [PubMed: 18178644]
68. Deng L, Fairbank NJ, Fabry B, Smith PG, Maksym GN. Am J Physiol Cell Physiol. 2004; 287:C440–448. [PubMed: 15070813]

69. Wolff L, Fernandez P, Kroy K. PLoS ONE. 2012; 7:e40063. [PubMed: 22815724]
70. Chaudhuri O, Parekh SH, Fletcher DA. Nature. 2007; 445:295–298. [PubMed: 17230186]

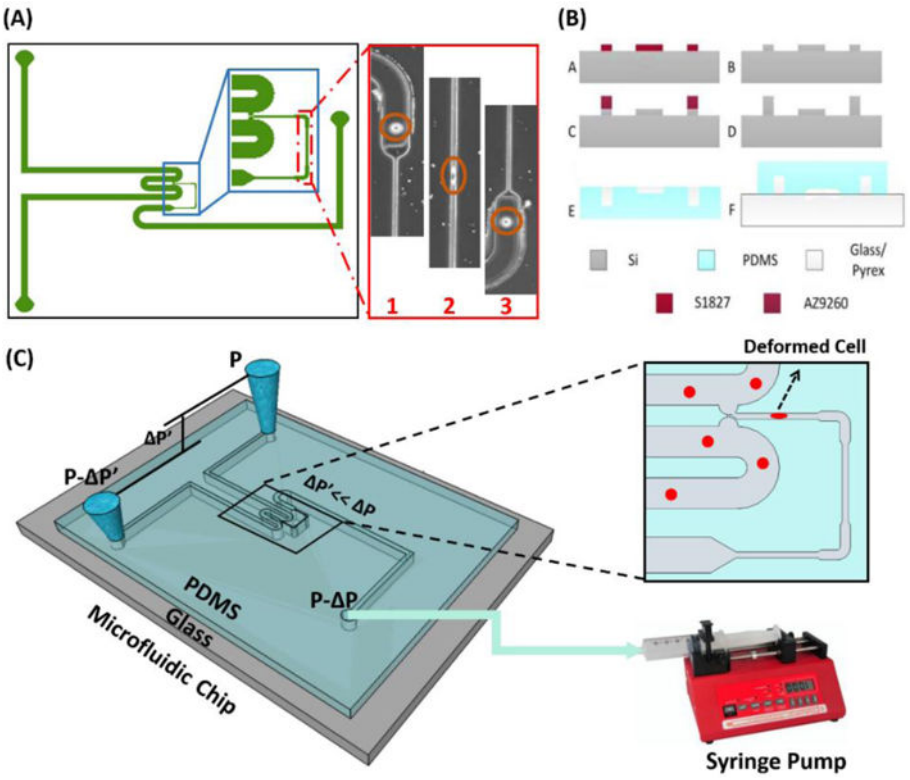

Figure 1.

A) Illustration of design, B) fabrication process flow, and C) schematic image of setup and operation principle of the iMECH analyzer.

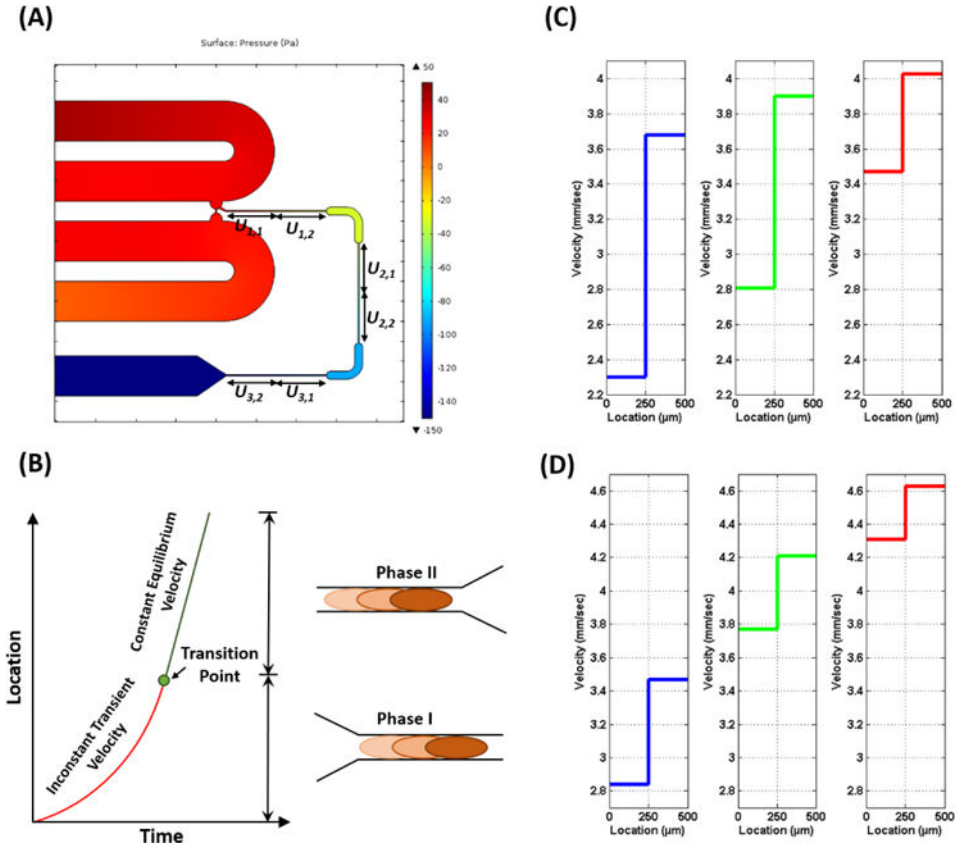

Figure 2.

A) The plot of pressure gradient in the microfluidic channels. B) The plot of the location versus time for a single cell traveling through a deformation channel. The average transient velocity and equilibrium velocity in the iterative deformation channels for a typical (C) non-metastatic cell (MCF10A) and (D) metastatic cancer cell (MDA-MB-231) cell.

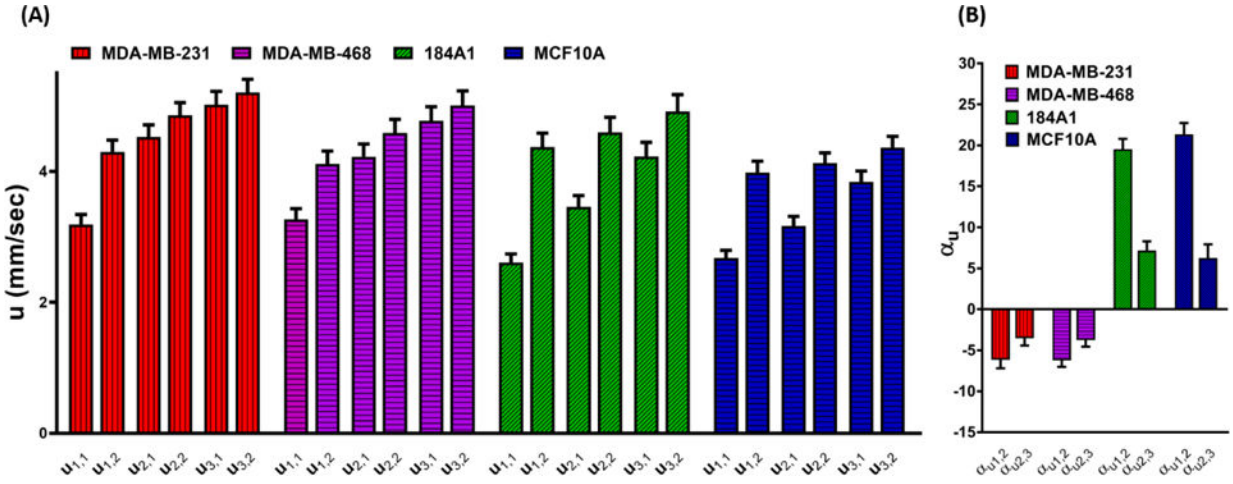

Figure 3.

A) Depiction of changes in the average transient ($u_{i,1}$) and equilibrium ($u_{i,2}$) velocities in the iterative deformation channels (i=1, 2, 3) for the four breast cell lines. B) Column bars of the calculated relative percentage change of velocities between each two successive deformation channels ($\alpha_{u1,2}$ and $\alpha_{u2,3}$) for the selected breast cell lines. The results are shown as mean ± standard error of mean (SEM) for at least n=100 cells of each cell line.

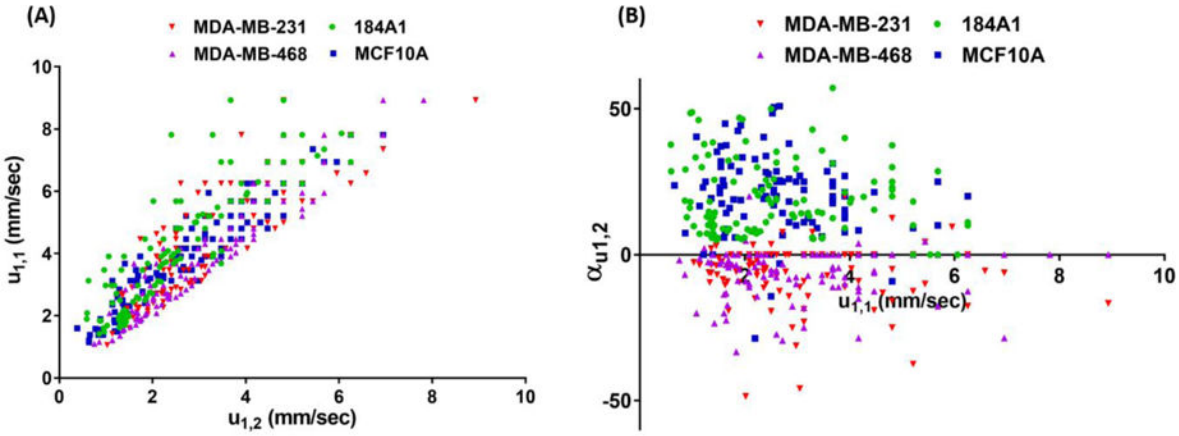

Figure 4.

A) Scatter plot of the first deformation channel's absolute transient ($u_{1,1}$) and equilibrium ($u_{1,2}$) velocities of breast cell lines. B) Scatter plot of the relative percentage change of velocity ($\alpha_{u1,2}$) vs. the first deformation channel's absolute transient velocity ($u_{1,1}$) provides a new bio-signature for single-cell level identification.

Table 1

Summary of previous works on single-cell biomechanical characterizations via microfluidic constriction channel based analyzers

Group	Targeted Cell Lines	Quantified Parameters	Method	Key Observation
Erickson et al.[24, 25]	MDA-MB-231 metastatic breast	Transit time	Multi-staged serial invasion channels (M.U.S.I.C.) device	The initial transit requires the longest time than the subsequent transits
Lim et al.[26]	MCF10-A benign, MCF-7 non-metastatic breast	Entry time, elongation index, transit velocity	A constriction microchannel	MCF10-A have longer entry but not travel times than MCF-7 with similar sizes
Vanapalli et al.[27]	Cancerous A172/1321N1, normal L0329/L036 glial	Elongation, pressure drop, speed, entry time	A microfluidic cell squeezer	Brain tumor cells take a longer time to squeeze and migrate more slowly than benign cells
Agah et al.[28]	MDA-MB-231 metastatic breast	Entry time, travel time	A constriction with two embedded Cr/Au electrodes	Nanoparticles-treated cells are significantly stiffer than untreated cells
Fabry et al.[29]	K562, MDA-MB-231, U2OS, HEK293T	Flow speed, cell deformation, entry time	Micro-constriction parallel arrays	A power law correlates entry time to driving pressure and cell size, and estimates cell elasticity & fluidity
Manalis et al.[10]	MEF fibroblast, cancer (T_{Met}, T_{nonMet}, H1650, H1975, HCC827), L1210 leukemia	Cell size/mass, entry velocity, transit velocity	A suspended microchannel resonator (SMR)	Changing the deformability of the cell alters the entry velocity, whereas changing the surface friction alters the transit velocity
Liu et al.[30]	Benign MCF-10A, metastatic MDA-MB-231, RPE epithelium	Cortical tension, Young's modulus	A microfluidic pipette array (μFPA)	The device captures stiffness of single cells and mechanical gating of mechanosensitive channels
Iqbal et al.[31]	Normal urothelial and T24 cancer bladder	Peak amplitude, translocation time	A 20 μm pore on oxide membrane	Tumor cells showed one order of magnitude shorter translocation time
Han et al.[32]	Breast cancer MCF-7, benign MCF-10A	Cell diameter, passage time	A micro-channel with real-time controllable gap	Size-independent cell deformability cytometry causes a much smaller degree of variation in passage times
Jensen et al.[33]	Hela cervical cancer	Cell volume, transit time	A constriction channel with electrodes	Hela cells have a faster transit time after treatment with latrunculin

Group	Targeted Cell Lines	Quantified Parameters	Method	Key Observation
				A and cytochalasin B
Sun et al.[34, 35]	MC-3T3 osteoblast, MLO-Y4 osteocyte	Transit time, cell elongation, aspiration length	A constriction channel with two Ag/AgCl electrodes	Osteoblasts have a larger cell elongation and transit time compared with osteocytes
Sun et al.[36]	Adult and Neonatal RBCs	Transit time	″	Adult compared with neonatal RBCs have distinct and lower transit time
Han et al.[37, 38]	Plasmodium falciparum infected RBCs	Transit velocity	A channel with triangular pillar array	Transit velocity of malaria infected RBCs decreases by 50% after treatment
Ma et al.[39–44]	Malaria infected/oxidized RBCs	Cortical tension Normalized position	A funnel channel chain pipette aspiration	Malaria infected/damaged RBCs show increased cortical tension and decreased deformability
Chiu et al.[45]	P. falciparum infected RBCs	Channel blockage	A constriction channel	Malaria decreases the deformability of infected RBCs
Rathod et al.[46]	P. falciparum infected RBCs	MCD: Minimum cylindrical diameter	Wedge-shaped micro-channels	Malaria infected RBCs show larger MCD
Suresh et al.[47]	Healthy RBCs	Stretch ratio, transit velocity, entrance/traversal/exit times	A pressure-control constriction	Experimental–computational analysis of the flow dynamics of RBCs
Kaneko et al.[48]	RBCs of healthy and a diabetes patient	Dimensionless stiffness DI index	A 4.0 μm microchannel	The proposed DI can significantly highlight the differences in stiffness of the healthy and diseased cells
Russell et al.[49]	P. vivax and P. falciparum RBCs	Normalized transit/recovery ratio	A 2.0 μm constriction	In contrast to P. falciparum-infeded, P. vivax-infected RBCs readily deform and recover a normal shape
Chang et al.[50]	Normal RBCs and cancerous (leukemia)	Transit velocity, elongation index, shape recovery time	A PDMS microchannel under optical pressure	A 3D distribution demonstrates the differences in deformability between two RBC types
Stone et al.[51]	Healthy RBCs, Healthy WBCs	Pressure-drop variation	A device with twin (comparator and test) channels	The device allows differentiation of cells with different mechanical properties or geometrical features

Group	Targeted Cell Lines	Quantified Parameters	Method	Key Observation
Theodoly et al.[11, 52]	THP-1 monocytic (WBCs) leukemia	Fluorescence microscopy	A sequential constriction device	F-actin mainly contributes to cell stiffness and bleb formation
Theodoly et al.[53]	″	Loss modulus	″	An apparent viscosity of single cells was estimated by numerical analysis
Fletcher et al.[54, 55]	WBCs with sepsis and leukostasis	Transit time	Parallel capillary-like micro-channels	Transit time of blood cells correlates with symptoms of diseases
Kamm et al.[56]	WBCs (neutrophils)	Entrance time, pseudopod projection time	A narrow PDMS capillary	Neutrophils deformation results in cytoskeletal remodeling, viscoelastic changes and pseudopod projection

Table 2

Percentage of tested single cells identified as metastatic cells via iMECH bio-signature ($\alpha_{u1,2}$) in mixtures of MDA-MB-231 and MCF10A cells with ascending ratio.

MDA-MB-231:MCF10A mixture ratio	% of cells predicted metastasis	% of cells identified metastasis via iMECH bio-signature
0:1	0%	7%
1:10	10%	15%
1:1	50%	59%
1:0.1	90%	87%
1:0	100%	95%